Spectroscopic Studies of 12-Oxo-5(12*H*)-naphthacenylidene and 7*H*-Benz[*de*]anthracen-7-ylidene in Shpolskii Matrixes at 5 K

M. Aloshyna and B. Kozankiewicz*

Institute of Physics, Polish Academy of Sciences, Al. Lotników 32/46, 02-668 Warsaw, Poland

Christopher M. Hadad,* John R. Snoonian, and Matthew S. Platz*

Department of Chemistry, The Ohio State University, Columbus, Ohio 43210

Received: November 29, 1999; In Final Form: February 15, 2000

The triplet−triplet fluorescence and fluorescence excitation spectra of two new, planar diaryl carbenes in *n*-hexane and *n*-heptane were studied at cryogenic temperatures. Fluorescence decays were fitted to three exponential functions. Fluorescence decays of 12-oxo-5(12*H*)-naphthacenylidene were sensitive to the presence of a magnetic field, and this dependence allowed the estimation of the zero field splitting parameters (*D*) of the excited triplet state of this compound, which were 0.037 ± 0.010 and 0.03 ± 0.015 cm^{-1} for the low- and high-energy sites, respectively. These results are corroborated by computational studies of the ground-state preferences and the triplet excitation energies.

I. Introduction

Carbenes play an important role in organic chemistry as short-lived intermediates because they are produced in many chemical reactions.[1] They can be generated from the appropriate diazo, diazirine, and/or ketene precursors by photolysis with visible or UV light. Experimental studies of reactive intermediates present a challenge because their concentration in either the gaseous or condensed phase at room temperature is extremely low. This problem can be avoided, however, by using matrix isolation techniques. In a cryogenic matrix, friction greatly restricts molecular motion and effectively eliminates intramolecular and intermolecular reactions. Thus, under these conditions it is possible to produce a relatively large and stable concentration of carbenes and study them for many days— in practice as long as the matrix is kept frozen. Thus, for 30 years diarylcarbenes have been studied by low-temperature EPR and fluorescence spectroscopy. These studies have contributed greatly to our current understanding of the structures of these species.[2]

Carbenes possess two nonbonding electrons and, depending on their molecular structure, may have either a triplet or singlet electronic ground state. Information about the geometry and electronic structure of triplet carbenes can be obtained by EPR and electronic absorption and emission spectroscopy of carbenes immobilized in matrix hosts.[2−4] In a low-temperature Shpolskii matrix, the $T_1 \rightarrow T_0$ fluorescence and $T_0 \rightarrow T_1$ fluorescence excitation spectra[4] are often composed of sharp, zero-phonon quasi-lines accompanied by broad phonon wings. These quasi-lines are inhomogeneously broadened due to the slightly different environments of the ensemble of carbenes produced in a polycrystalline matrix, providing a convenient situation for hole-burning studies using highly selective irradiation with a narrow-band ring dye laser. These types of hole-burning experiments on the (0,0) line of a $T_0 \rightarrow T_1$ fluorescence excitation spectrum were recently performed on 2-naphthylphenylcarbene (2-NPC)[5,6] and 2,2-dinaphthylcarbene (22-DNC)[7] dispersed in *n*-hexane at 1.7 K. These studies enabled the deduction of the zero-field splitting (ZFS) parameters of both the T_0 and T_1 states and provided information about energy relaxation in the carbenes of interest. 2-NPC and 22-DNC exist in several rotameric forms which complicates their spectroscopy. Therefore, in the present work, we have synthesized and undertaken spectroscopic studies of two new, planar and rigid relatives of 2-NPC, which are shown below:

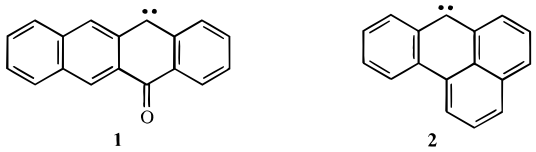

1 **2**

II. Experimental Section

A. Spectroscopy. Carbenes **1** and **2** were obtained "in situ" by the photolysis of the corresponding diazo precursors dispersed in a Shpolskii matrix of either *n*-hexane or *n*-heptane at 5 K. The 366 nm line, isolated by appropriate filters from the spectrum of a mercury lamp, was used to photolyze the diazo precursors. Before being inserted into the liquid helium cryostat, all samples were degassed by the "freeze−pump−thaw" technique. Samples were annealed overnight, and the cryostat was warmed slowly to approximately 100 K (in the dark) and subsequently cooled back the next day to a temperature slightly above that of boiling liquid helium.

The fluorescence and fluorescence excitation spectra of the carbenes were measured using two different experimental techniques. In the photon counting configuration, the samples were excited either with the 366 nm line isolated from the spectrum of an HBO200 mercury lamp or with the light emitted by a Coherent 700 dye laser pumped by a mode-locked Coherent Antares 76-YAG laser. In the latter case a laser was scanned within the lasing frequency range of the Rhodamine 6G dye, i.e., between 562 and 625 nm. Emission spectra were observed at a right angle to the photolysis source using a 0.25 m Jarrel-Ash monochromator and an EMI 9659 photomultiplier, cooled

10.1021/jp994183r CCC: $19.00
Published on Web 03/28/2000

to −20 °C and operating in the photon counting mode. A LightScan PC card was used as the pulse counting electronics and as the master of the experiment. In the photon sampling configuration, the excitation source was a Lambda Physik FL 1001 dye laser pumped by an LPX 100 excimer laser. Different lasing dyes were used for the wavelength ranges of interest: Rhodamine B, 598−625 nm; Rhodamine 101, 615−655 nm; and DCM, 645−690 nm. Fluorescence light was detected with the aid of an EMI 9659 photomultiplier and a Stanford Research SR250 boxcar averager connected with the previously mentioned PC card.

Fluorescence decays were measured using the "time-correlated" single photon counting technique. The samples were excited in this case by the previously mentioned Coherent laser system, which provided light pulses of a 20 ps pulse width and 3.8 MHz repetition rate. Start and stop signals were detected by an avalanche photodiode and a Hamamatsu R28090-07 microchannel plate photomultiplier, respectively. A Tennelec TC 454 quad constant fraction discriminator, a TC 864 time to amplitude converter, and a Nucleus PCA-II multichannel analyzer PC card were used. The estimated time resolution of this setup was about 50 ps.

B. Synthesis. *Preparation of 5,12-(H)-Naphthacenone.* In a 250 mL round-bottomed flask was suspended 4.0 g (15.5 mmol) of 5,12-naphthacenequinone (Aldrich) and 8.0 g (67.4 mmol) of granular tin metal in 100 mL of glacial acetic acid. The suspension was heated to reflux, at which time the quinone dissolved and the solution's color became deep red. After 90 min at reflux, the solution was yellow brown, and 10 mL of concentrated HCl was carefully added. The solution was then cooled to room temperature. A brown precipitate was collected by vacuum filtration. To the brown filtrate was added 50 mL of water to give additional brown solid. The solids were dissolved in a minimum amount of benzene and passed through a short column of silica gel using benzene as the eluant. The product eluted with an $R_f = 0.54$ (benzene), and the fractions containing the product were concentrated by rotary evaporation. The compound was a yellow powder (3.0 g) with mp = 194−196 °C (lit.[8] 195−196 °C).

Preparation of 12-Diazo-5-naphthacenone. In a 250 mL round-bottomed flask was suspended 1.0 g (4.10 mmol) of ketone in 130 mL of acetonitrile. To the suspension was added 1.08 g (4.51 mmol) of *p*-acetamidobenzenesulfonyl azide. The mixture was stirred for 5 min, and then 0.406 g (4.10 mmol) of triethylamine was added in one portion. The flask was wrapped in foil and stirred at ambient temperature for 24 h at which time about 10% unreacted ketone remained. The now brown solution was concentrated to a volume of about 80 mL, and 1.0 mL additional triethylamine was added. After an additional 12 h, the mixture was concentrated (no heat) under vacuum to a volume of about 20 mL, and the brown precipitate was collected by vacuum filtration. Following washing with cold acetonitrile and drying, the brown-red solid proved to be 0.804 g of the desired diazo compound, which decomposes at 205 °C. IR: (CCl_4) 2052 (C═N_2), 1678 (C═O) cm^{-1}.

Preparation of 7H-Benz[de]anthracen-7-one Hydrazone. In a 100 mL round-bottomed flask was placed 1.00 g (4.35 mmol) of 7*H*-benz[*de*]anthracen-7-one (Aldrich), 15 mL of hydrazine hydrate, and 1.80 g of zinc chloride in 30 mL of ethylene glycol. The mixture was refluxed for 12 h, cooled, and poured into 100 mL of water. The aqueous solution was extracted with 4 × 50 mL dichloromethane; the total organic layer was dried over Na_2SO_4 and concentrated by rotary evaporation to give an orange oil. The oil was chromatographed on silica gel using 98:2 CH_2Cl_2:CH_3CN ($R_f = 0.47$) as the eluant and yielded 0.915 g of the hydrazone as a yellow solid. Recrystallization from hexane gave 0.594 g of **3** as fine yellow needles (mp = 126° C). IR: 3405 (NH), 1617 (C═N) cm^{-1}.

Preparation of 7-Diazo-7H-benz[de]anthracene. To 0.100 g (0.410 mmol) of hydrazone in 10 mL of tetrahydrofuran in a 25 mL round-bottomed flask was added 1.0 g of anhydrous Na_2SO_4. After stirring for 10 min, 0.264 g (1.14 mmol) of Ag_2O was added in one portion. The solution was stirred in the dark for 1 h, and then the inorganic salts were removed by vacuum filtration. The THF was removed from the filtrate by rotary evaporation (no heat) to give a brown-purple solid that was washed with 2 mL of cold Et_2O. The dark purple solid (0.080 g) proved to be the desired diazo compound, which decomposed at 96° C. IR: (CCl_4) 2037 (C═N_2) cm^{-1}.

C. Computational Methods. Calculations were performed with Gaussian 94 and 98.[9] The 6-31G(d) and 6-31G(d,p) basis sets were utilized with 6 D Cartesian functions.[10] All geometries were fully optimized with the Becke three-parameter exchange functional along with the Lee−Yang−Parr correlation functional (B3LYP),[11] as implemented in Gaussian.[9] The minima were verified via vibrational frequency calculations and possessed the correct number of real vibrational frequencies. The calculated zero-point vibrational energies were scaled by 0.9806.[12] Thermal corrections to 298 K (1 atm pressure) were utilized as generated by Gaussian (but without any scaling of the vibrational frequencies).

The vertical triplet excited-state energies were generated with the time-dependent density functional theory method[13] using the UB3LYP/6-31G(d,p) reference wave function for the corresponding triplet ground state. The vertical excitation energy calculations utilized the UB3LYP/6-31G(d) geometry for the triplet ground state. The TD-UB3LYP calculations were performed as implemented in Gaussian 98.[9b]

III. Results and Discussion

A. Summary of Computational Results. An immediate concern was the nature of the ground state for carbenes **1** and **2**. Computational methods often have difficulty with an adequate description of the triplet state with unrestricted Hartree−Fock-based methods due to spin contamination issues.[10] However, density functional theory (DFT) methods[14] have proven to be less susceptible to spin contamination for aromatic systems.[15] We have therefore utilized B3LYP/6-31G(d) optimized geometries for carbenes **1** and **2** for the singlet (RB3LYP) and triplet (UB3LYP) states. The energetic results are listed in Table 1, along with two other carbenes (**3** and **4**), which are of similar structure. In general, the triplet state is heavily favored by >6

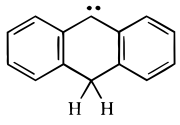

3

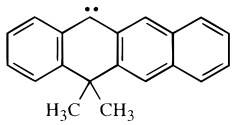

4

kcal/mol for carbenes **1** and **2** and slightly less favored for structures **3** and **4**. Some geometric information for **1** and **2** is presented in Figure 1 for the S_1 and T_0 states. The most striking differences between the singlet and triplet structures are the much longer C−C (carbene center) bond lengths as well as the smaller C−C−C bond angle at the carbene center in S_1. Specifically, in S_1 for **1**, the C−C bond lengths are 1.453 and 1.460 Å, while the corresponding values in T_0 are 1.401 and 1.403 Å. For **2**, S_1 has values of 1.449 Å (both), and T_0 has

TABLE 1: Calculated Singlet−Triplet Splittings for Carbenes 1−4[a]

	B3LYP/6-31G(d)			B3LYP/6-31G(d,p)// B3LYP/6-31G(d)		
carbene	ΔE_{BW}	ΔH_{298}	ΔG_{298}	ΔE_{BW}	ΔH_{298}	ΔG_{298}
1	8.8	9.1	8.6	8.9	9.2	8.7
2	6.7	7.3	7.6	6.9	7.4	7.7
3	2.3	2.6	4.7			
4	3.0	3.5	3.9			

[a] In units of kcal/mol. The triplet state is the ground state for **1**−**4**. The ΔE_{BW} energies are at the bottom of the well and do not include ZPE corrections. ΔH_{298} corresponds to relative enthalpies at 298 K, including a scaled ZPE correction. ΔG_{298} corresponds to relative free energies at 298 K, including a scaled ZPE correction.

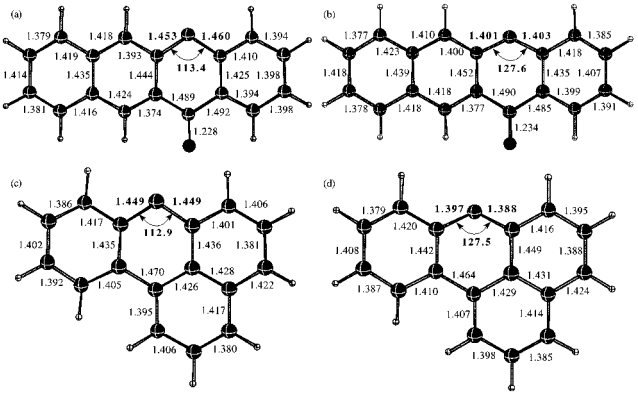

Figure 1. Selected geometric parameters (B3LYP/6-31G(d)) for **1** S_1 (a), **1** T_0 (b), **2** S_1 (c), and **2** T_0 (d). Bond distances are in Å, and bond angles are in degrees.

bond lengths of 1.397 and 1.388 Å for the C−C(carbene) bond lengths. Also, the C−C−C bond angles are about 15° larger for the T_0 states.

There are limited data available with which to assess the reliability of the computational method employed herein for the prediction of singlet−triplet energy separations of diarylcarbenes. The most relevant study is that of Zhu et al.[16] who used density functional theory to predict that the triplet state of 2-naphthyl(carbomethoxy)carbene lies 4.52 kcal/mol below the lowest singlet state of this carbene. Toscano and co-workers[17] demonstrated that the triplet is indeed the ground state of this carbene in Freon solution, but by only 0.2 kcal/mol. In this case, it is not known if the disagreement between theory and experiment is due to a shortcoming of the computational method or is a consequence of the fact that the calculations relate to the gas phase and the measurement was made in solution. This is the only case in which a singlet−triplet gap has been measured directly in solution. Others have tried to derive such values from kinetic studies but this approach remains controversial.[18] Given that the singlet−triplet separations of **1** and **2** are larger than the 4.52 kcal/mol of the benchmark study it seems reasonable to conclude from the calculations that these carbenes have triplet ground states.

Using the UB3LYP reference wave function for the ground state, we have also calculated the vertical excitation energies from the T_0 ground state to the excited triplet states (Table 2). At the TD-UB3LYP/6-31G(d,p) level, the lowest vertical excitation energy is 16 394 cm^{-1} (2.03 eV) for **1** and 18 354 cm^{-1} (2.28 eV) for **2**. The $T_0 \rightarrow T_1$ (vertical) excitations for **1** and **2** are HOMO → LUMO transitions and are of $\pi \rightarrow \pi^*$ character. The energetic results are very consistent with the adiabatic energies that were experimentally determined (see below). However, due to program limitations in Gaussian,[9] we were not able to optimize the excited triplet state in order to calculate the adiabatic transition energy. We should also point out that the nonbonding σ orbital in **1** is not perturbed by the presence of the O atom.

TABLE 2: Calculated Time-Dependent UB3LYP/6-31G(d,p) Vertical Excitation Energies for the Triplet States of 1 and 2[a]

state	symmetry	transition energy (eV, cm^{-1})	osc str
		Carbene 1	
T_0	A″		
T_1	A′	2.03 (16 394)	0.0004
T_2	A″	2.28 (18 371)	0.0000
T_3	A′	2.49 (20 059)	0.0062
		Carbene 2	
T_0	A″		
T_1	A′	2.28 (18 354)	0.0001
T_2	A′	2.81 (22 696)	0.0011
T_3	A′	2.97 (23 989)	0.0078

[a] The optimized UB3LYP/6-31G(d) geometry for T_0 was used in each case.

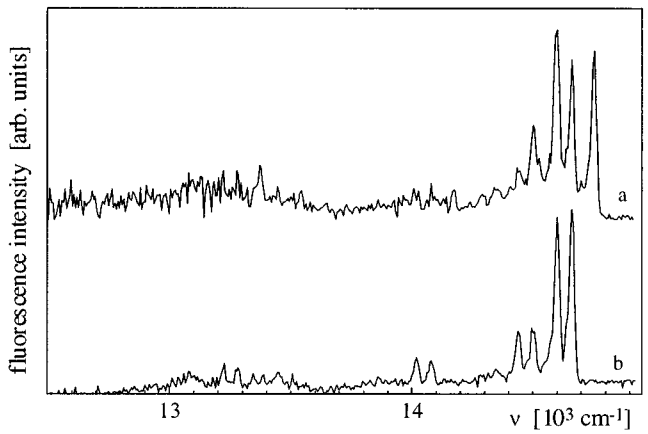

Figure 2. Fluorescence spectra of **1** in *n*-hexane at 5 K observed (a) just after photolysis and (b) the next day after the overnight annealing procedure. The wavelength of excitation light in both cases was 366 nm.

B. Fluorescence and Fluorescence Excitation Spectra of 1. The fluorescence spectrum of **1** in a Shpolskii matrix of *n*-hexane at 5 K, excited by the 366 nm line to an excited triplet state, is shown in Figure 2. It is a characteristic feature of Shpolskii matrices that the spectrum is composed of narrow lines originating from several matrix sites. Just after photolysis, the (0,0) fluorescence lines of different sites due to **1** are located at 14 750, 14 668, and 14 587 cm^{-1}. The high-energy site disappears after annealing overnight. Parts a and b of Figure 3 show that the fluorescence and fluorescence excitation spectra of **1** in both sites that remain after the annealing process are separated under conditions of selective laser excitation. The respective (0,0) fluorescence origins are located at 14 669 and 14 587 cm^{-1} (681.65 and 684.7 nm, respectively) and those of fluorescence excitation spectra at 14 660 and 14 603 cm^{-1}, respectively. The spectral resolution of the fluorescence spectra were limited by the monochromator (half-bandwidth above 30 cm^{-1}), whereas the fluorescence excitation spectra were measured with the laser spectral resolution of 0.2 cm^{-1}. It is clear that the (0,0) origins of fluorescence and fluorescence excitation spectra coincide and therefore can be identified with the zero-phonon lines. Thus, the system seems to be a good candidate for forthcoming hole-burning experiments.

The fluorescence spectra of **1** in *n*-heptane, before and after the overnight annealing, are shown in Figure 4. After annealing,

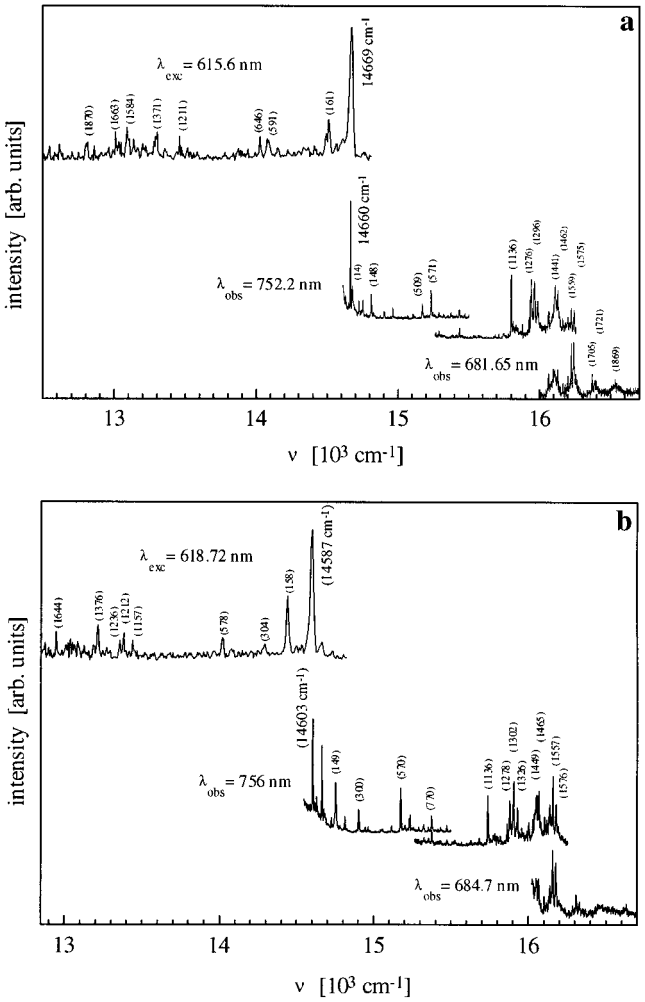

Figure 3. Fluorescence and fluorescence excitation spectra of (a) the high-energy site and (b) the low-energy site of **1** in *n*-hexane at 5 K, observed after the sample was annealed. The wavelengths of excitation (λ_{exc}, in the case of the fluorescence spectrum) and wavelengths of observation (λ_{obs}, in the case of the fluorescence excitation spectrum) are indicated close to the corresponding spectrum. The numbers in parentheses indicate the vibrational frequencies (given in cm^{-1}) obtained with respect to the (0,0) origins of both sites.

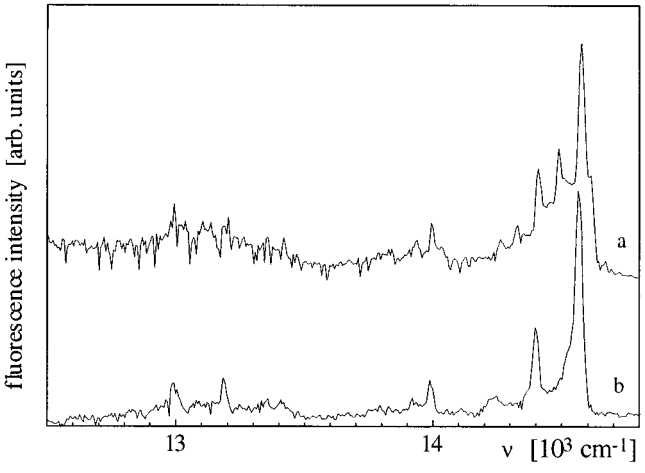

Figure 4. Fluorescence and fluorescence excitation spectra of **1** in *n*-heptane at 5 K observed (a) before and (b) after the sample was annealed. The wavelength of excitation, in both cases, was 366 nm.

the spectrum is simpler and a single site is observed. As shown in Figure 5, the (0,0) fluorescence and fluorescence excitation lines can be considered to be coincident because they are located

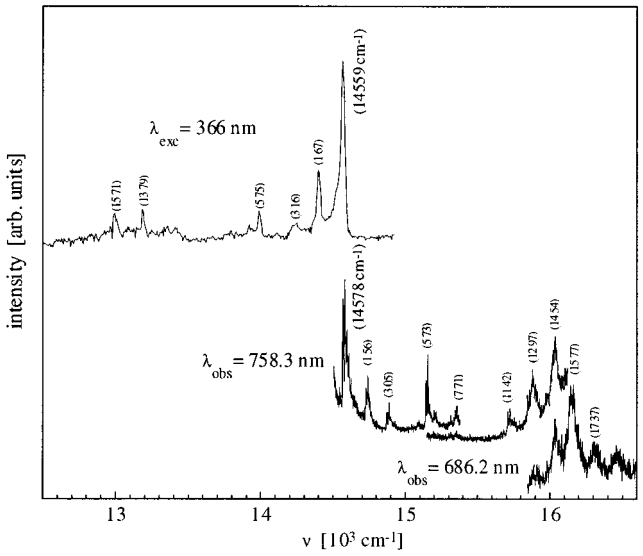

Figure 5. Fluorescence and fluorescence excitation spectra of **1** in *n*-heptane at 5 K, observed after the sample was annealed. The wavelengths of excitation (λ_{exc}, in the case of the fluorescence spectrum) and wavelengths of observation (λ_{obs}, in the case of the fluorescence excitation spectrum) are indicated close to the corresponding spectra. The numbers in parentheses indicate the vibrational frequencies (given in cm^{-1}) estimated with respect to the frequency of the (0,0) origin.

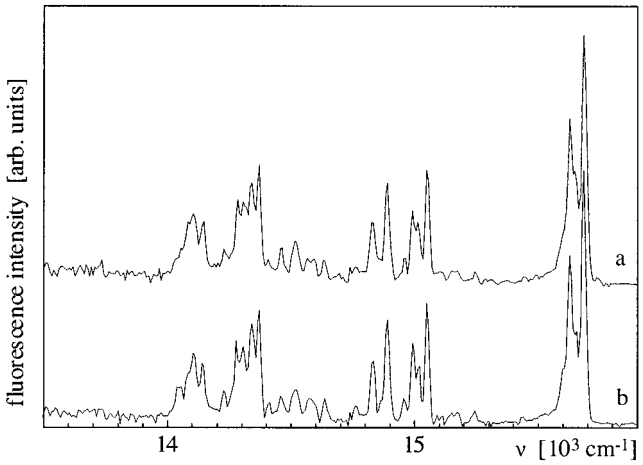

Figure 6. Fluorescence and fluorescence excitation spectra of **2** in *n*-hexane at 5 K observed (a) before and (b) after the sample was annealed. The wavelength of excitation was 366 nm.

at 14 559 and 14 578 cm^{-1}, respectively. A close inspection of the (0,0) fluorescence excitation line (obtained with the superior resolution provided by the laser) shows, however, that it is composed of several narrow lines located ±12 cm^{-1} around the most intense one, thus suggesting the presence of several sites containing the carbene, which differ slightly in energy.

C. Fluorescence and Fluorescence Excitation Spectra of 2. The fluorescence spectrum of **2** in *n*-hexane at 5 K is composed of narrow lines and does not change after overnight annealing, as shown in Figure 6. The main fluorescence lines, located at 15 680 and 15 622 cm^{-1}, belong to two different sites of **2** in the matrix, as is clearly seen from the analysis of the spectra presented in Figure 7. The corresponding fluorescence excitation lines located at 15 673 and 15 615 cm^{-1} are the origins of the progression of vibronic components, having the frequencies of 527, 616, 650, 785, and 1002 cm^{-1}. The computed vibrational frequencies of **1** and **2** are available as

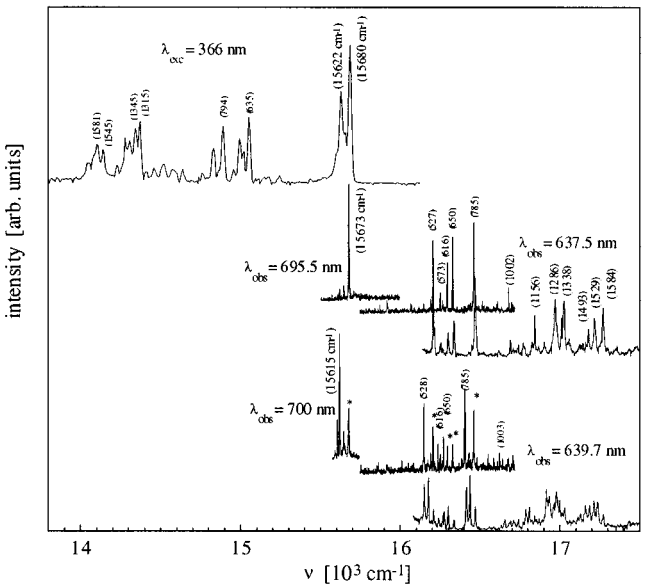

Figure 7. Fluorescence and fluorescence excitation spectra of **2** in *n*-hexane at 5 K, observed after the sample was annealed. The fluorescence excitation spectra of both main sites (with their (0,0) lines at 15 673 and 15 615 cm^{-1}) are observed under the condition of selective laser excitation. The wavelengths of excitation (λ_{exc} = 366 nm, in the case of the fluorescence spectrum) and wavelengths of observation (λ_{obs}, in the case of the fluorescence excitation spectrum) are indicated close to the corresponding spectra. The numbers in parentheses indicate the vibrational frequencies (given in cm^{-1}) estimated with respect to the frequency of the (0,0) origin of both sites. The fluorescence excitation spectrum of the high-energy site contains some bands (labeled with an asterisk, *) belonging to the spectrum of the low-energy site.

Supporting Information. Unfortunately, it is not possible to assign the observed vibrations because of the multitude of frequencies predicted for the large molecules of this work.

D. Fluorescence Decays. Fluorescence decays for both carbenes were studied in *n*-hexane at 5 K. The decay curves are shown in Figures 8 and 9. All of the decays were nonexponential, as observed previously for several other carbenes.[4,7,19,20] This has been interpreted as a result of different intersystem crossing rates from the three triplet sublevels of the T_1 state, manifested by a three-exponential fluorescence decay. Since the transition moments are spin independent, the radiative rate constants for the three spin sublevels should be equal and the excitation pulse should equally populate the three spin sublevels of the T_1 state. Thus, the experimental decays are expected to be a sum of three exponential decays with the same preexponential factors. (The above consideration does not take into account the Boltzmann population of the spin sublevels of the T_0 state via the intersystem crossing channel. Furthermore, we assume that thermal equilibrium is not established in the excited T_1 state because of long spin−lattice relaxation times at 5 K and the short lifetime of this state, and all three spin sublevels decay independently.)

We fitted the decays with a three-exponential function with the same preexponential factors and optimized four fitting parameters (three decay times and an amplitude). The crucial conditions required to obtain successful fitting (convolution with the excitation pulse) were high-quality decay curves (to fulfill this requirement, we collected the decay curves up to 10^4 counts in maximum) and a very precise estimation of the baseline. Under these conditions, the iterative, nonlinear least-squares fitting program found the best approximation of the decays with the component decay times presented in Table 3. We estimate that the accuracy of our fitting procedure is better than ±0.2 ns, as given by the maximal difference between the component decay times obtained from different experimental data.

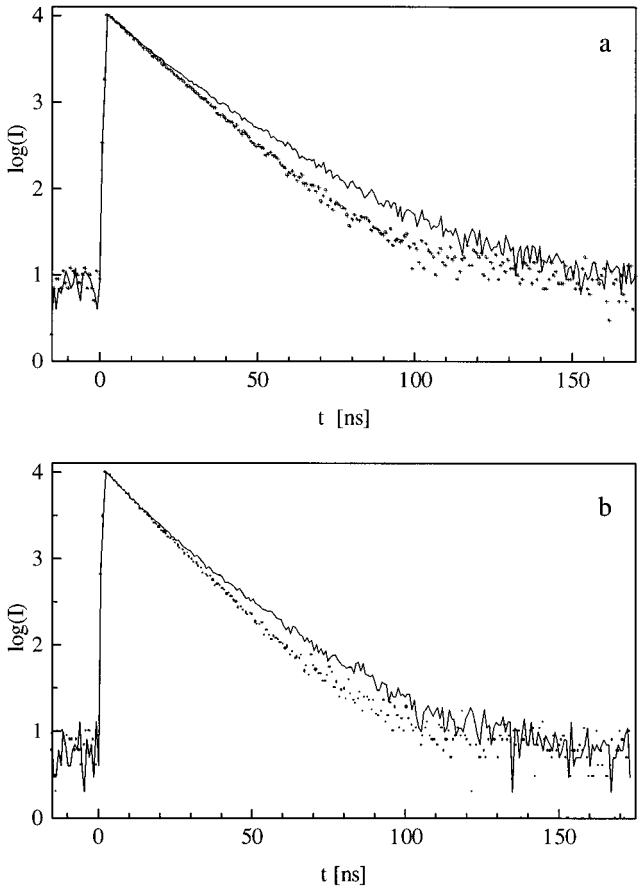

Figure 8. Fluorescence decays of **1** in *n*-hexane at 5 K in the absence (solid lines) and in the presence of 330 G of magnetic field (open circles): (a) λ_{exc} = 16 220 cm^{-1}, λ_{obs} = 14 669 cm^{-1}, corresponds to the high-energy site of **1**; (b) λ_{exc} = 16 160 cm^{-1}, λ_{obs} = 14 587 cm^{-1}, corresponds to the low-energy site.

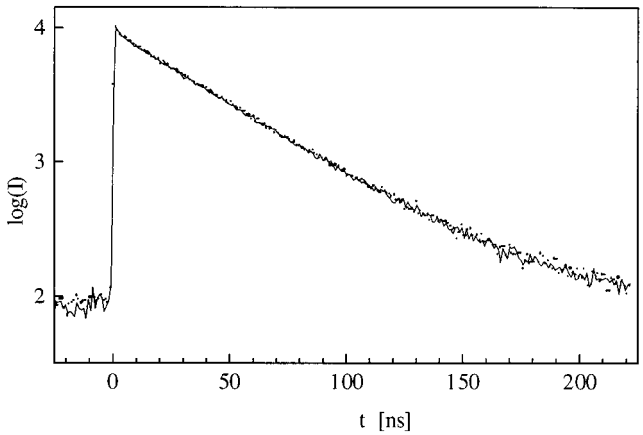

Figure 9. Fluorescence decays of **2** in *n*-hexane at 5 K in the absence (solid lines) and in the presence of 330 G of magnetic field (open circles). The decays correspond to the high-energy site of **2**, λ_{exc} = 16 458 cm^{-1}, λ_{obs} = 15 680 cm^{-1}.

It is interesting to note that carbene **2** has two equal decay times and a slightly smaller value for the third decay time. The relaxation channel that can lead to different decay components of the T_1 state is intersystem crossing to the singlet manifold. Thus, we conclude that it is weak for **2**. This observation also corroborates the conclusions from our recent hole burning experiments,[21] which showed that the dominant relaxation of the T_1 state proceeds via internal conversion.

TABLE 3: Best Fit Parameters Obtained When Fitting Fluorescence Decays by the Decay Dependence $F(t) = A(\exp(-t/\tau_1) + \exp(-t/\tau_2) + \exp(-t/\tau_3))$, Where τ_1, τ_2, and τ_3 Are the Component Decay Times and A Is the Common Amplitude of the Decay Components

carbene	ν_{exc} (cm^{-1})	ν_{obs} (cm^{-1})	τ_1 (ns)	τ_2 (ns)	τ_3 (ns)
1	16 160	14 587	7.2	12.0	18.0
	16 220	14 669	7.8	14.2	20.9
2	16 458	15 680	36.4	44.5	44.5
	16 400	15 622	31.2	42.9	43.0

Upon application of a static magnetic field (up to 330 G), the fluorescence decay of **1** was altered whereas that of **2** was not (see Figures 8 and 9). The modification of the decay curves upon application of the magnetic field was previously interpreted as a consequence of the Zeeman mixing of the wave functions of the T_1 state spin sublevels having different nonradiative decay rates via the intersystem crossing relaxation channel. This process averages decay components. It is therefore obvious that in the case of **2**, where all of the decay components are nearly the same (see the data given in Table 3), the magnetic field mixing cannot lead to any visible change of the fluorescence decay curve. In the case of **1**, where the slow decay rate is about 3 times smaller than that of the quickly decaying spin sublevel, the magnetic field mixing can effectively change the total decay shape.

In the presence of a weak magnetic field H (when $g\beta H \ll D_1$, here D_1 is the zero-field splitting parameter of the T_1 state), the formula for the rate of the effective slow decay component $\langle k_{xH} \rangle$, is given by [22,23]

$$\langle k_{xH} \rangle = k_x + {}^2/_3\,(g\beta H/D_1)^2((k_y + k_z)/2 - k_x)$$

where k_x, k_y and k_z are the total decay rates (reciprocals of the corresponding decay components) from the X, Y, and Z spin sublevels in the absence of the magnetic field. In the above expression, every quantity except D_1 can be obtained from the fluorescence decay experiment, and therefore this expression can be used to estimate the D_1 value. Using this approach we found that $D_1 = 0.037 \pm 0.010$ cm^{-1} for the low-energy site of **1** and $D_1 = 0.03 \pm 0.015$ cm^{-1} for the high-energy site of **1**.

The ZFS parameter D is proportional to $\langle 1/r^3 \rangle$, where r is the average separation between the two unpaired electrons. The D_1 values obtained are similar to those found for the excited T_1 state of several other carbenes[4,7] and correspond to substantial delocalization of one of the unpaired electrons onto the aromatic ring (occupying a π^* orbital), whereas the second electron remains localized on the carbenic center in an in-plane σ orbital.

IV. Conclusions

Two new, planar and rigid diaryl carbenes, 12-oxo-5(12*H*)-naphthacenylidene (**1**) and 7*H*-benz[*de*]anthracen-7-ylidene (**2**), were synthesized and studied by optical spectroscopic techniques. The fluorescence spectra are consistent with each carbene having a triplet ground state. This is in agreement with the singlet−triplet energy splittings calculated with density functional theory methods.

Fluorescence and fluorescence excitation spectra of these carbenes in low-temperature (5 K) Shpolskii matrixes of *n*-hexane and *n*-heptane were composed of narrow lines attributed to the zero-phonon components. These systems are therefore good candidates for hole-burning studies presently underway. These carbenes resided in multiple sites inside the Shpolskii matrixes, which were manifested by the observation of multiple sets of (0,0) origins in the fluorescence and fluorescence excitation spectra. The energy separation of the different sites in the same (annealed) matrix did not exceed 80 cm^{-1}.

Fluorescence decays were fitted by the dependence of the three exponentials with common amplitude. Each exponent corresponds to one spin sublevel of the T_1 state and thus describes excitation energy relaxation from this sublevel, which can proceed via radiative and internal conversion channels (with rates equal for the three sublevels) and via intersystem crossing (with rates which can be different for the three spin sublevels). Application of a static magnetic field modified the fluorescence decay of **1** (but did not alter that of **2**) and allowed an estimation of the zero-field splitting parameter $D_1 = 0.037 \pm 0.010$ cm^{-1} (and 0.03 ± 0.015 cm^{-1} for the second site) of the excited T_1 state of carbene **1**. A small D_1 parameter value is typical for triplet carbenes where one of unpaired electrons occupy a π^* orbital of the aromatic ring and the second electron is in an in-plane σ orbital localized on the carbenic center.

Acknowledgment. Support of this work in Columbus, OH, by the National Science Foundation is gratefully acknowledged by M.S.P. (CHE-9613861) and C.M.H. (CHE-9733457). We also acknowledge support from the Ohio Supercomputer Center where some of the calculations reported here were completed. J.R.S. gratefully acknowledges support by an Ohio State postdoctoral fellowship.

Supporting Information Available: The computed vibrational frequencies of **1** and **2**. This information is available free of charge via the Internet at http://pubs.acs.org.

References and Notes

(1) (a) Kirmse, W. *Carbene Chemistry*; Academic Press: New York, 1964. (b) *Carbenes*; Jones, M., Jr., and Moss, R. A., Eds; Wiley: New York, 1973 and 1975; Vols. I and II. (c) Wentrup, C. *Reactive Molecules*; Wiley: New York, 1984.

(2) (a) Trozzolo, A. M.; Wasserman, E. In *Carbenes*; Moss, R. A., Jones, M., Jr., Eds.; Wiley: New York, 1975; Vol. II, p 185. (b) Sander, W.; Bucher, G.; Wierlacher, S. *Chem. Rev.* **1993**, *93*, 1583.

(3) Closs, G. L. In *Carbenes*; Moss, R. A., Jones, M., Jr., Eds.; Wiley: New York, 1975; Vol. II, p 159.

(4) Migirdicyan, E.; Kozankiewicz, B.; Platz, M. S. In *Advances in Carbene Chemistry*; U. Brinker, U., Ed.; JAI Press Inc., 1998; Vol. 2, p 97.

(5) Kozankiewicz, B.; Bernard, J.; Migirdicyan, E.; Orrit, M.; Platz, M. S. *Chem. Phys. Lett.* **1995**, *245*, 549.

(6) Kozankiewicz, B.; Bernard, J.; Migirdicyan, E.; Orrit, M.; Platz, M. S. *Mol. Cryst. Liq. Cryst.* **1996**, *283*, 191; **1996**, *291*, 143.

(7) Kozankiewicz, B.; Aloshyna, M.; Gudmundsdottir, A.; Platz, M. S.; Orrit, M.; Tamarat, Ph. *J. Phys. Chem. A* **1999**, *103*, 3155.

(8) Saeva, F. D.; Breslin, D. T.; Luss, H. R. *J. Am. Chem. Soc.* **1991**, *113*, 5333.

(9) (a) Frisch, M. J.; Trucks, G. W.; Schlegel, H. B.; Gill, P. M. W.; Johnson, B. G.; Robb, M. A.; Cheeseman, J. R.; Keith, T.; Petersson, G. A.; Montgomery, J. A.; Raghavachari, K.; Al-Laham, M. A.; Zakrzewski, V. G.; Ortiz, J. V.; Foresman, J. B.; Peng, C. Y.; Ayala, P. Y.; Chen, W.; Wong, M. W.; Andres, J. L.; Replogle, E. S.; Gomperts, R.; Martin, R. L.; Fox, D. J.; Binkley, J. S.; Defrees, D. J.; Baker, J.; Stewart, J. J. P.; Head-Gordon, M.; Gonzalez, C.; Pople, J. A. *Gaussian 94*, Revision D.3; Gaussian, Inc.: Pittsburgh, PA, 1995. (b) Frisch, M. J.; Trucks, G. W.; Schlegel, H. B.; Scuseria, G. E.; Robb, M. A.; Cheeseman, J. R.; Zakrzewski, V. G.; Montgomery, J. A., Jr.; Stratmann, R. E.; Burant, J. C.; Dapprich, S.; Millam, J. M.; Daniels, A. D.; Kudin, K. N.; Strain, M. C.; Farkas, O.; Tomasi, J.; Barone, V.; Cossi, M.; Cammi, R.; Mennucci, B.; Pomelli, C.; Adamo, C.; Clifford, S.; Ochterski, J.; Petersson, G. A.; Ayala, P. Y.; Cui, Q.; Morokuma, K.; Malick, D. K.; Rabuck, A. D.; Raghavachari, K.; Foresman, J. B.; Cioslowski, J.; Ortiz, J. V.; Stefanov, B. B.; Liu, G.; Liashenko, A.; Piskorz, P.; Komaromi, I.; Gomperts, R.; Martin, R. L.; Fox, D. J.; Keith, T.; Al-Laham, M. A.; Peng, C. Y.; Nanayakkara, A.; Gonzalez, C.; Challacombe, M.; Gill, P. M. W.; Johnson, B.; Chen, W.;

Wong, M. W.; Andres, J. L.; Gonzalez, C.; Head-Gordon, M.; Replogle, E. S.; Pople, J. A. *Gaussian 98*, Revision A.6; Gaussian, Inc.; Pittsburgh, PA, 1998.

(10) Hehre, W. J.; Radom, L.; Schleyer, P. v. R.; Pople, J. A. *Ab initio Molecular Orbital Theory*; John Wiley & Sons: New York, 1986.

(11) (a) Becke, A. D. *Phys. Rev. A* **1988**, *38*, 3098. (b) Becke, A. D. *J. Chem. Phys.* **1993**, *98*, 5648. (c) Lee, C.; Yang, W.; Parr, R. G. *Phys. Rev. B* **1988**, *37*, 785.

(12) Scott, A. P.; Radom, L. *J. Phys. Chem.* **1996**, *100*, 16502.

(13) (a) Bauernschmitt, R.; Ahlrichs, R. *Chem. Phys. Lett.* **1996**, *256*, 454. (b) Stratmann, R. E.; Scuseria, G. E.; Frisch, M. J. *J. Chem. Phys.* **1998**, *109*, 8218.

(14) (a) Labanowski, J. W.; Andzelm, J. *Density Functional Methods in Chemistry*; Springer: New York, 1991. (b) Parr, R. G.; Yang, W. *Density Functional Theory in Atoms and Molecules*; Oxford University Press: New York, 1989.

(15) See for example: Barckholtz, C.; Barckholtz, T. A.; Hadad, C. M. *J. Am. Chem. Soc.* **1999**, *121*, 491−500 and references therein.

(16) Zhu, Z.; Bally, T.; Stracener, L.; McMahon, R. *J. Am. Chem. Soc.* **1999**, *121*, 2863.

(17) Wang, Y.; Yuzawa, T.; Hamaguchi, H.; Toscano, J. P. *J. Am. Chem. Soc.* **1999**, *121*, 2875.

(18) Griller, D.; Nazran, A.; Scaiano, J. C. *J. Am. Chem. Soc.* **1984**, *106*, 198.

(19) Després, A.; Lejeune, V.; Migirdicyan, E.; Admasu, A.; Platz, M. S.; Berthier, G.; Pariser, O.; Flament, J. P.; Baraldi, I.; Momicchioli, F. *J. Phys. Chem*. **1993**, *97*, 13358.

(20) Kozankiewicz, B.; Després, A.; Lejeune, V.; Migirdicyan, E.; Olson, D.; Michalak, J.; Platz, M. S. *J. Phys. Chem.* **1994**, *98*, 10419.

(21) Kozankiewicz, B.; Aloshyna, M.; Sienkiewicz, A.; Orrit, M.; Tamarat, Ph.; Hadad, C. M.; Snoonian, J. R.; Platz, M. S. *J. Phys. Chem. A*, submitted.

(22) Lejeune, V.; Després, A.; Migirdicyan, E. *J. Phys. Chem.* **1990**, *94*, 8861.

(23) Després, A.; Lejeune, V.; Migirdicyan, E.; Platz, M. S. *J. Phys. Chem.* **1992**, *96*, 2486.